Clays and Clay Minerals, Vol. 68, No. 4:347–360, 2020

TRANSFORMATION OF MAGNESITE TO SEPIOLITE AND STEVENSITE: CHARACTERISTICS AND GENESIS (ÇAYIRBAĞI, KONYA, TURKEY)

MEFAİL YENİYOL *

[1]Department of Geology, Istanbul University-Cerrahpaşa, 34850 Avcılar, Istanbul, Turkey

Abstract—Çayırbağı magnesite is one of numerous magnesite deposits occurring throughout Turkey. In this deposit, sepiolite and newly found stevensite occur locally as two daughter minerals formed from magnesite. The sepiolite and stevensite show distinctive compositions and modes of formation compared to those described in the literature. The objective of the current study was to characterize these minerals by means of mineralogic, thermal, structural, geochemical, and textural analyses and to describe their mechanisms of formation. The geology, mineralogy, and geochemistry were examined by field work followed by X-ray diffraction (XRD), Fourier-transform infrared spectroscopy (FTIR), scanning electron microscopy (SEM), differential thermal (DTA), and thermogravimetric (TG) analyses. Chemical analyses were performed by means of electron microprobe (EMPA), inductively coupled plasma-optical emission spectrometry (ICP-OES), and laser ablation inductively coupled plasma-mass spectrometry (LA-ICP-MS). The XRD analyses showed that the d_{110} of the sepiolite was at 12.64 Å and at 13 Å after air-drying and ethylene-glycol solvation, respectively. Identification of the sepiolite as sepiolite-13 Å was supported by FTIR and TG-DTA data. Chemical analyses showed an ideal composition with a structural formula of $(Ca_{0.05}K_{0.02})(Mg_{7.79}Al_{0.10}\square_{0.11})Si_{12}O_{30}(OH)_4$. Stevensite displayed distinctive results for XRD, FTIR, and thermal characteristics. The structural formula of stevensite was: $(Ca_{0.01}Na_{0.20}K_{0.04})(Mg_{1.90}Al_{0.30}Fe^{3+}_{0.37}Ti_{0.01}\square_{0.43})(Si_{3.93}Al_{0.07})O_{10}(OH)_2$, indicating a layer charge arising mainly from octahedral sheets. Field and SEM observations demonstrated that sepiolite was formed from magnesite by transformation via a dissolution–precipitation mechanism. Descending surface waters were responsible for this transformation. Thick magnesite veins were partly replaced whereas in thin veins sepiolite replaced the overall mass. Both surface waters with high Si, low Al and Fe activities, and pH values of 8–9.5 were responsible for sepiolite formation. Stevensite was formed similarly to sepiolite with respect to the mechanism and parent mineral under permanent groundwater; where both Si, Fe, Al activities and pH (>9.5) were high.

Keywords—Magnesite · Replacement · Sepiolite · Stevensite · Transformation

INTRODUCTION

Sepiolite and stevensite are authigenic Mg-rich clay minerals having different structural organizations. According to numerous published papers, these minerals form in a variety of geological environments: in Si- and Mg-rich alkaline lakes and shallow seas via direct precipitation from alkaline or saline water (Papke 1972; Tettenhorst and Moore 1978; Khoury et al. 1982; Eberl et al. 1982; Galan and Castillo 1984; Ece and Çoban 1994; Karakaş and Kadir 1998; Singer et al. 1998; Pozo and Casas 1999; Buey et al. 2000; Mayayo et al. 2000; Kadir and Akbulut 2001; Kadir et al. 2002; Akbulut and Kadir 2003; Karakaya et al. 2004; Furquim et al. 2008; Galan and Pozo 2011; Yeniyol 1992, 2007, 2012, 2014; Kadir et al. 2016, 2017; and many others), transformation from precursor Mg-bearing silicate phases (Stoessell and Hay 1978; Chahi et al. 1997; Pozo and Casas 1999; Cuevas et al. 2003; Hover and Ashley 2003; Yeniyol 1997, 2012, 2014, and others), hydrothermal alteration of magmatic rocks (Faust and Murata 1953; Randal 1959; Imai et al. 1970; Post 1984; April and Keller 1992; İrkeç and Ünlü 1993), and weathering of mafic and ultramafic rocks (Kodama et al. 1988; Yalçın and Bozkaya 2004; Christidis and Mitsis 2006).

To the knowledge of the author, no mention is made in the literature of sepiolite and stevensite being formed from magnesite. An occurrence of the sepiolite, meerschaum, was reported by Yeniyol and Öztunalı (1985) to have formed by replacement of magnesite. A vein-like sepiolite occurrence was discovered at Çayırbağı (Yeniyol 1986) confirming the previous findings. This occurrence was described in a short note and so knowledge of sepiolite being formed by replacement of magnesite was limited. Because of its mode of occurrence and distinct origin, other researchers interpreted the genesis of this well known meerschaum sepiolite (Yeniyol 1993; Ece and Çoban 1994; Ece 1998; Kadir et al. 2016). During the present reexamination of this vein-like sepiolite, a Mg-smectite was discovered for the first time displaying distinct chemical composition and genetic relationships with magnesite. The purpose of the current research was to investigate the unusual formation mechanisms and genesis of sepiolite and newly found stevensite, and to document in greater detail the characteristics of these Mg-clay minerals.

GEOLOGICAL SETTING

The sepiolite occurrence is located at western Çayırbağı village, ~20 km from Konya City (Fig. 1a). The basement lithology of the area comprises units ranging in age from Mesozoic to Cenozoic. The Mesozoic is represented by Lower Triassic detrital sediments and dolomitic limestone, by Middle Triassic–Upper Jurassic crystallized limestone, and by Lower–Upper Cretaceous pelagic mudstone as well as radiolarian chert interbedded with pelagic carbonates and limestone. The Hatip ophiolite complex and Çayırbağı ophiolite consist of

* E-mail address of corresponding author: yeniyolm@istanbul.edu.tr

DOI: 10.1007/s42860-020-00083-9

pyroxenite altered to serpentinite and of gabbro dykes. These complexes were emplaced as large overthrust slabs over the older lithologies during the Upper Cretaceous. These were covered by Neogene lacustrine sediments containing conglomerate, clayey limestone, and limestone overlying the older rocks discordantly (Tuncay 2000).

The Çayırbağı ophiolite contains magnesite deposits in the uppermost parts. These deposits occurred as both veins and stockworks. The veins of magnesite are 0.2 to 5–6 m thick whereas stockwork magnesite is represented by intersecting veins 5–20 cm thick. Magnesite was formed by the interaction of CO_2-rich surface waters with serpentinite during the ophiolite emplacement (Yeniyol 1982; Tuncay 2000). The magnesite looks white and massive and contains either moderately large and hard silica components or soft and friable substances. Compressional tectonic events affected the magnesite veins leading to faulting, brecciation, and even mylonitization. Magnesite was also found locally at the base of Neogene sediments which consist of marl and limestone. Magnesite appeared in the base of these sediments as short and thin undulating veins as well as nodules which were formed by chemical precipitation from lake water.

Sepiolite and Mg-smectite were formed as late-stage phases under supergene conditions. They appeared locally as stockwork magnesite. Sepiolite occurs as thin, undulating veins <20 cm thick. These veins intersect each other displaying a stockwork structure inherited from the pre-existing magnesite (Fig. 1b,c). In these veins, magnesite has been replaced entirely by sepiolite (Yeniyol 1986). Sepiolite veins commonly show desiccation cracks perpendicular to vein surfaces and which are traversed by thin quartz and sepiolite veinlets in many cases. Weak tectonic movements caused short displacements along these cracks (Fig. 1b,c).

A 40–45 cm thick magnesite vein appears at the same location. This vein contains both magnesite and sepiolite, providing a helpful example of their genetic origin (Fig. 1d). The lower part consists of magnesite. Based on its physical properties (color, texture, density, hardness, and fracturing), the sepiolite contents were noted to increase gradually from bottom to top and from the middle toward the vein surfaces. Due to the presence of sepiolite, rare desiccation cracks appear perpendicular to the vein toward the top.

Smectite was found ~5 m inside a 50 m research gallery (Fig. 1b). Here, a 45–50 cm thick and almost vertical vein of magnesite occurs. The vein has been broken by tectonic activity into two parts. In an inclined lower part, magnesite was ground and mylonitized along a zone between the two parts of the vein. Smectite occupied the overall mylonitized zone and appeared as a 10–15 cm thick horizontal and laminated layer showing sharp boundaries from the magnesite. Lateral extensions continue toward both sides aligning with the vein surface. Similarly, the stevensite layer showed sharp contacts with the serpentinite wall rock.

MATERIALS AND METHODS

Sepiolite occurred in hand specimens as planar laths and flakes up to 1.5 cm long and traversed by 0.5 mm thick quartz veinlets. It was porous, lightweight, and white colored. When wet, it is light beige in color with a soap-like appearance. In wet samples of stevensite, the laminae became more prominent and the material becomes soft and easily carved.

Several samples were collected from the magnesite-sepiolite vein, including pure sepiolite and smectite. Five representative samples were collected. Three samples were from a sepiolite-bearing magnesite vein and used to trace compositional changes from magnesite to sepiolite (samples Ç1, Ç2, Ç3). The other two samples were collected from a pure sepiolite vein (Ç4) at the face of a trench, and from smectite (Ç5) which occurred inside the gallery (Fig. 1b,c,d).

Preliminary powder XRD analyses revealed that sepiolite and Mg-smectite samples were monomineralic and pure in the raw state. Therefore, all analyses were performed on bulk samples of sepiolite, smectite, and mixtures of sepiolite and magnesite. The XRD analyses were carried out using random powders of both sepiolite and smectite as well as oriented samples of smectite. Because the smectite samples were found to be resistant to dispersion in water, in order to prepare oriented samples, raw material was soaked in water overnight, ground gently under water using an agate mortar and pestle, dispersed alternately by mechanical stirring and ultrasonic treatment, and then were settled by centrifugation. Oriented samples were prepared by smearing clay residue onto glass slides. Oriented samples which were air-dried, ethylene glycol-solvated, and heated (550°C for 2 h) then solvated again with EG were used to determine the nature of the smectite (Christidis and Koustopoulou 2013). The XRD analyses were done utilizing a Philips PW 3020 diffractometer (Almelo, The Netherlands) with CuKα radiation and a graphite diffracted-beam monochromator, operating at 40 kV and 20 mA, in the range 3–65°2θ with a step size of 0.04°2θ min^{-1}.

The DTA and TG analyses (TA SDT Q600, New Castle, Delaware, USA) were done simultaneously on sepiolite and smectite samples in the 25–1000°C range using 20 mg of sample under a 100 mL/min air flow and a 10°C/min heating rate. Al_2O_3 was used as the reference material.

The FTIR analyses were carried out on sepiolite and stevensite samples using an ATI Unicam Mattson 1000 FTIR spectrometer (Burladingen, Germany). Samples were first diluted with KBr at a ratio of 1:200 and subsequently were compressed in the form of discs. Then they were scanned in the frequency range of 4000 to 450 cm^{-1}.

The SEM analyses were performed on gold-coated chips using an FEI Quanta FEG 450 SEM instrument (Hillsboro, Oregon, USA).

Smectite samples displayed a laminated structure (particularly when wet) appearing in alternating light to dark brownish hues. To remove the free iron oxide, the dithionite-citrate (Merck, Darmstadt, Germany) procedure was used (Mehra and Jackson 1960). Free Fe was determined from the supernatant solution.

In order to detect the chemical differences and possible changes in Fe content perpendicular to alternating laminae of smectite, chemical analyses were carried out of six spots on a dry polished sample. Analyses were performed using an

https://doi.org/10.1007/s42860-020-00083-9 Published online by Cambridge University Press

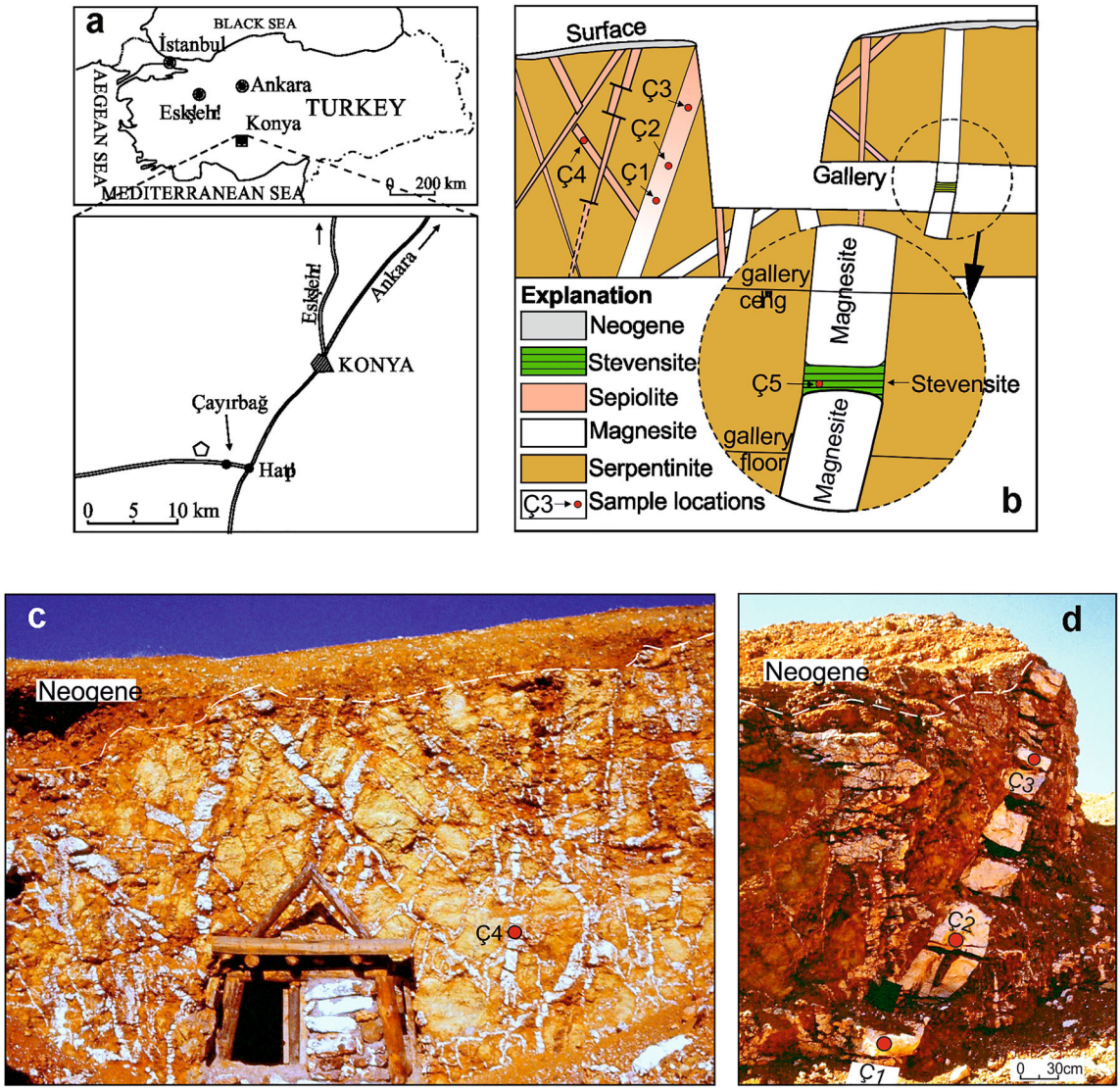

Fig. 1. **a** Location map of study area; **b** schematic sketch showing field relationships and sample locations; **c** general view of sepiolite veins on the face of a trench; **d** magnesite+sepiolite vein and sample locations

electron microprobe (Jeol-733, Tokyo, Japan) equipped with three wavelength dispersive spectrometers (WDS) under vacuum, at a 15 kW accelerating voltage with a 1.99×10^{-8} A probe current in 30 μm diameter and the Benson Albee program.

Chemical analysis was done using ICP-OES (Perkin Elmer Avio 200 ICP-OES, New Boston, Massachusetts, USA). Analyses were performed after $LiBO_2$ fusion for all major oxides (SiO_2, TiO_2, Al_2O_3, Fe_2O_3, MnO, MgO, CaO, K_2O, Na_2O, and P_2O_5). Trace element and rare-earth element concentrations were determined using inductively coupled plasma-mass spectrometry (ICP-MS, Perkin Elmer Nexion 2000, New Boston, Massachusetts, USA) combined with a laser ablation system (ESI NWR 213, Huntingdon, UK). Laser spot sizes of 110 μm were utilized in analysis. NIST SRM610, SRM612, and BCR2 glass disks were used as external standards. For each of the analyses, ~20 s of background signal was collected before the initiation of the ablation process. Sample ablation times were selected as 50 s with a laser repetition rate of 5 Hz; helium was the carrier gas. Data reduction for all analyses was achieved using *ICPMSDataCal* (Liu et al. 2008). The structural formulae of the sepiolite and smectite were determined from ICP-OES analyses of the pure samples (confirmed by XRD) of sepiolite and smectite.

RESULTS

XRD

Sepiolite is characterized by an intense 110 peak at 12.64 Å with a 1.25°2θ full width at half maximum (FWHM) and characteristic remaining reflections (Fig. 2). Reflections which typically occur at 12–19°2θ were very weak. Also, reflections

https://doi.org/10.1007/s42860-020-00083-9 Published online by Cambridge University Press

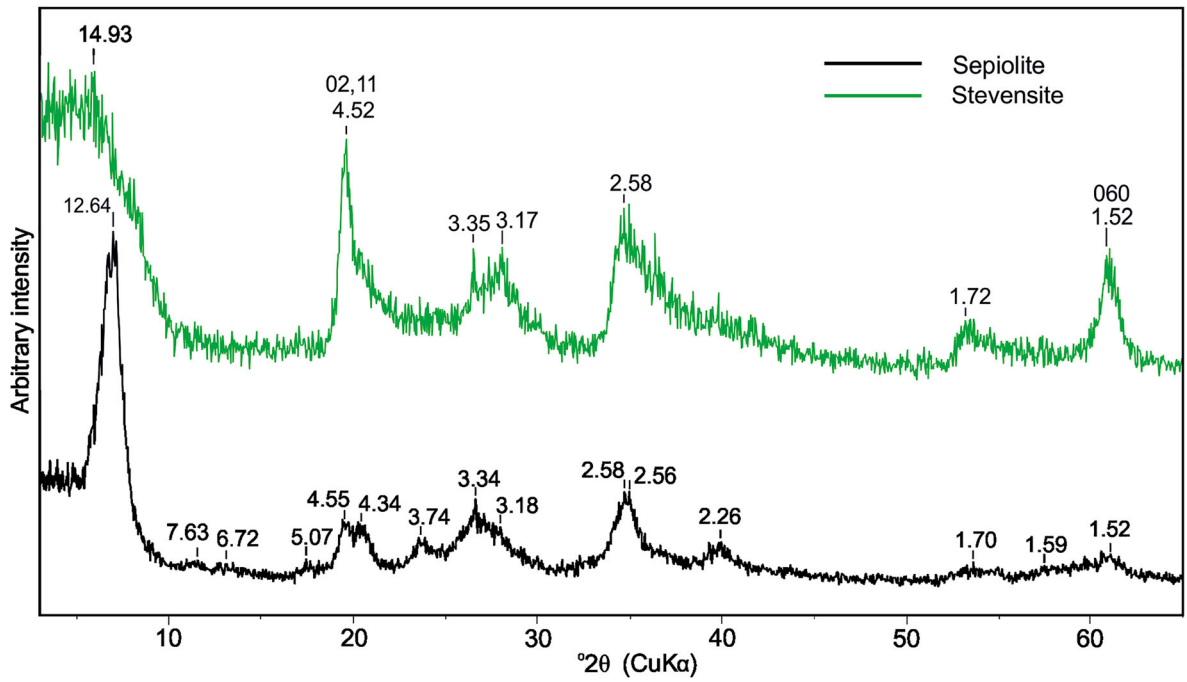

Fig. 2. XRD patterns of randomly oriented samples of sepiolite and stevensite

at 19–21°2θ were of equal intensity. Those reflections between 26 and 31°2θ were not well resolved, appearing as a convoluted peak with two maxima at 3.3 and ~3.2 Å. In addition, some of the remaining reflections were different both in terms of their shapes and *d* values. The large *d* value of the first reflection and the characteristic other reflections indicated that the sepiolite is poorly ordered and similar to that described by Yeniyol (2014) as sepiolite-13 Å. The oriented and air-dried sample was dominated by a broad and intense 110 peak which shifted to 13 Å after EG solvation and contracted to 10.7 Å after heating at 600°C (Yeniyol 1986).

In the XRD pattern of a randomly oriented sample of stevensite, the basal reflection 001 was broad and asymmetric, and appeared at ~15 Å (Fig. 2). A 02,11 reflection occurred as a two-dimensional *hk* band due to the turbostratic structure of this mineral. A single and sharp 060 reflection appeared at 1.52 Å, indicating the trioctahedral nature.

In an oriented and air-dried sample, 001 occurs as a broad (with 4.2°2θ FWHM), symmetric, and strong reflection at 14.7 Å (Fig. 3). The mean crystallite thickness calculated from the Scherrer equation was 1.98 nm. After solvation with ethylene glycol (EG), this reflection shifted to 18.3 Å with a small saddle at the low-angle side. It appeared as a symmetric, intense, and broad peak with 2°2θ FWHM, giving a mean crystallite thickness of 4.15 nm. The higher-order reflections of stevensite appeared at 9.2, 5.7, 4.5, and 3.4 Å, displaying a rational series. After heating at 550°C for 2 h, the 001 peak shifted to 9.7 Å, indicating a talc-like phase formed due to the collapse of the Mg-smectite structure. In the case of heating to 550°C and subsequent EG solvation, the position of the 001 reflection (9.7 Å) did not change. According to the method proposed by Christidis and Koutsopoulou (2013) for identifying Mg-smectites, the smectite present was identified as stevensite.

FTIR Spectra

The FTIR spectrum of sample Ç4 was typical of poorly ordered sepiolite (Fig. 4) (Yeniyol 2014). In the region 3700–3000 cm^{-1}, spectra of sepiolite showed two bands at 3566 and 3443 cm^{-1}, corresponding to OH-stretching of

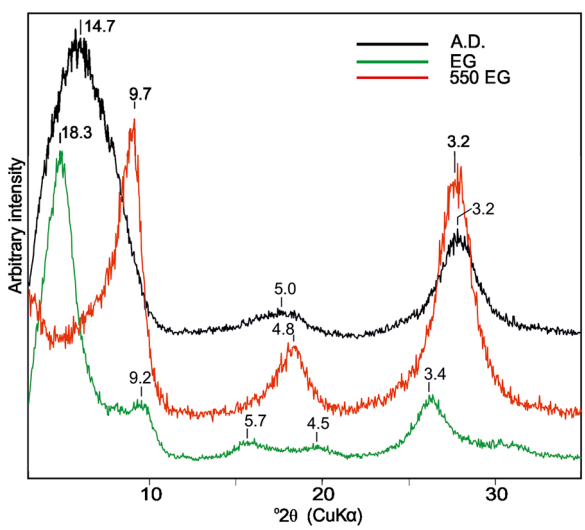

Fig. 3. XRD patterns of oriented samples of stevensite (Ç5). AD, air-dried; EG, solvated with ethylene glycol; 550EG, heated at 550°C then solvated with ethylene glycol

https://doi.org/10.1007/s42860-020-00083-9 Published online by Cambridge University Press

bound water and zeolitic water, respectively. The absorption band of the bending vibrations of the bound water molecules occurred at 1660 cm^{-1} (Frost et al. 1998, 2001). A weak band at 1380 cm^{-1} was found due to the bound water coordinated to Mg in the octahedral sheet (Sabah and Çelik 2002; Wouters et al. 2010). The weak band at 1208 cm^{-1} was attributed to Si–O–Si stretching between alternate ribbons (Suarez and Garcia-Romero 2006). An intense band at 1020 cm^{-1} corresponded to Si–O stretching. The positions of the Mg–OH bending vibrations appeared at 784 cm^{-1}, 690 cm^{-1}, and 653 cm^{-1}. In addition, a bending band occurred at 476 cm^{-1}.

The FTIR spectrum of sample Ç5 (Fig. 4) was characteristic of Mg-smectites (Yeniyol 2007, 2014) with two shoulders and a weak band occurring in order at 3680, 3626, and 3468 cm^{-1}. The first two bands correspond to structural hydroxyls whereas the third is attributed to the OH-stretching vibration of adsorbed water (Imai et al. 1970; Elton et al. 1997; Buey et al. 2000; Benhammou et al. 2009). The bending vibration of water molecules appeared at 1647 cm^{-1}. A strong and sharp absorption band occurred at 1022 cm^{-1} corresponding to Si–O stretching. In addition, two bands at 668 cm^{-1} and 462 cm^{-1} corresponded to Si–O–*R* vibrations where *R* = Mg, Fe, or Al (Christidis and Mitsis 2006).

Thermal Analyses

The DTA curve of the sepiolite showed the first endothermic peak at 88°C which was due to the loss of zeolitic water (Fig. 5a). Two broad and weak endothermic peaks occurred at 294°C and 430°C, corresponding to the loss of first and second halves of coordinated water, respectively. Removal of coordinated water in these two steps resulted in folding of the sepiolite structure and formation of sepiolite anhydride (Nagata et al. 1974; Serna et al. 1975; Rautureau and Mifsud 1977; Yeniyol 2014). A broad endothermic peak at 758°C was attributed to the loss of the hydroxyl groups. Finally, a sharp exothermic peak at 842°C indicated the collapse of sepiolite structure and the formation of enstatite.

The water loss was continuous for sepiolite, with four identifiable steps (Nagata et al. 1974; Serna et al. 1975; Frost and Ding 2003). The first water loss at 25–154°C (13.0 wt.%) belonged to both hygroscopic and zeolitic waters (Fig. 5a). The first half of the coordination water was rather weakly bonded in the structural channels and released from 154 to 335°C (3.0 wt.%). The loss of the second half occurred between 335 and 548°C (2.8 wt.%). The remaining weight loss was due to structural dehydroxylation from 548 to 836°C (3.0 wt.%). The total weight loss from the sample calculated from the TG curve was 21.8 wt.%.

The DTA and TG curves of stevensite (Fig. 5b) revealed a first endothermic peak at 95°C that corresponded to the loss of absorbed water. The second and third endothermic peaks were broad and weak, appearing at 215°C and 270°C, respectively. These peaks were assigned to the loss of interlayer water in two sequential steps. After a diffuse and inclined endothermic peak at ~485°C, which was attributed to the loss of the remaining interlayer water in close coordination with interlayer cations, a sharp endothermic peak at 815°C corresponded to the loss of hydroxyls (Imai et al. 1970; Yeniyol 2007, 2014). The exothermic peak at

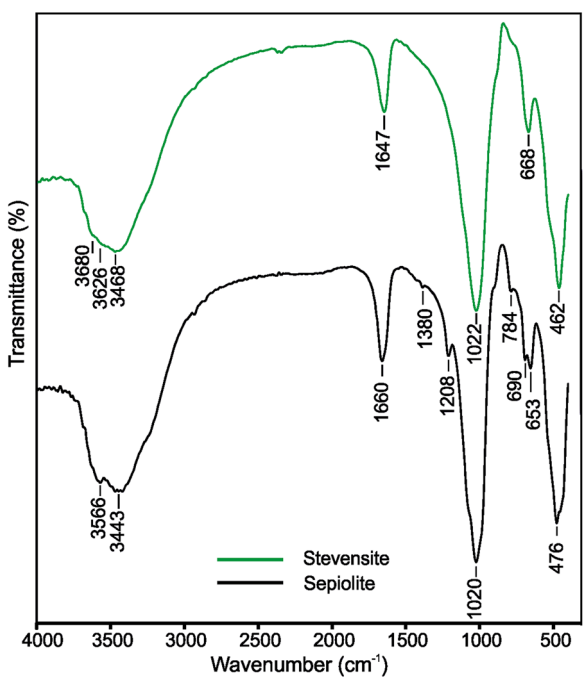

Fig. 4. FTIR spectra of sepiolite and stevensite

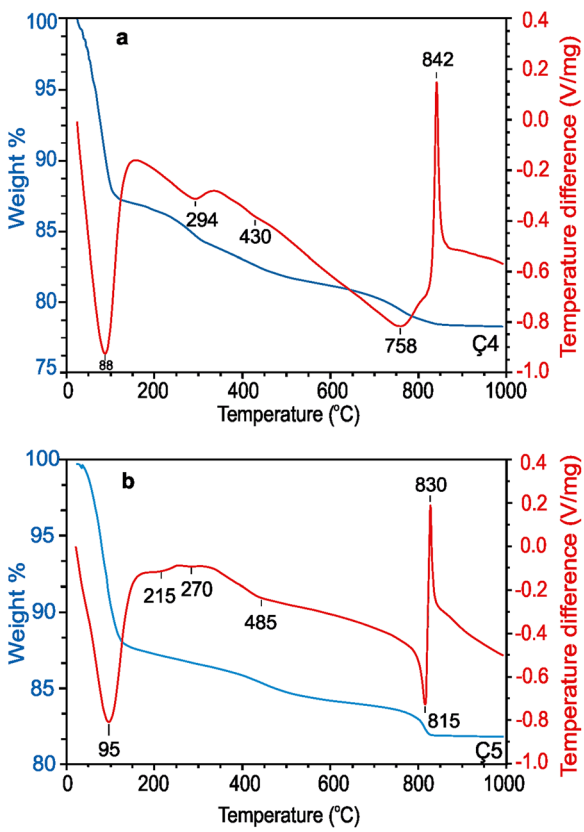

Fig. 5. DTA and TG curves of **a** sepiolite and **b** stevensite

https://doi.org/10.1007/s42860-020-00083-9 Published online by Cambridge University Press

830°C indicated the collapse of the stevensite structure and the probable formation of an augite-like pyroxene.

Weight losses corresponding to adsorbed water, interlayer water, and structural hydroxyl groups of stevensite occurred in the order: 24–173°C (3.0 wt.%), 173–615°C (3.3 wt.%), and 615–830°C (2.2 wt.%). The total weight loss was 17.7 wt.%.

SEM Analyses

Samples were collected from a vein where sepiolite and magnesite are found together (denoted as magnesite+sepiolite). The sepiolite/magnesite ratio increased from base to top (Ç1–Ç3) of the vein. Sepiolite appeared as straight, delicate fibers and planar structures in the interstitial space, parallel to the crystal faces enveloping the magnesite rhombs (Fig. 6 Ç1,2,3). Dissolution of magnesite was followed by the formation of sepiolite as crusts covering and embracing the magnesite crystals (Fig. 6Ç1a–2b). Where magnesite crystals were consumed as a whole, sepiolite appeared as crusts enclosing the voids with rhombic shapes and displaying encrustation pseudomorphs (Fig. 6Ç1a,b, Ç3a). In some magnesite crystals, transformation was incomplete, leading to magnesite crystal relics remaining within some voids (Fig. 6Ç1b, Ç3a,b). The traces of subsequent replacement events appeared as relict concentric crusts in some places (Fig. 6Ç1a). Sepiolite was formed mostly in interstitial spaces, but it was also found filling the veinlets (Fig. 6 Ç1c, Ç3c). In these veinlets, it appeared as parallel, fine fibers or fibers exceeding 50 μm as well as flakes.

Pure sepiolite made up the overall mass, showing a net structure (Fig. 7 Ç4a–Ç4d). It formed the walls of the voids displaying rhombic shapes. This demonstrated that precursor magnesite crystals were consumed entirely, leaving behind the voids as sepiolite pseudomorphs after magnesite. Sepiolite was also formed as a filling in submicroscopic desiccation cracks (Fig. 7 Ç4d).

Stevensite occurred in the form of fine, uneven flakes with slightly undulated edges surrounding the voids. In some cases, they are fairly flat and in 2–3 μm sized flakes which developed parallel to the surfaces of the laminae (Fig. 7Ç5c,d). Voids showed random spatial distribution, irregular shapes, and subrounded sizes ranging from 0.1 to 1.5 μm. These features indicated the presence of a fine-grained and irregularly shaped pre-existing substance. In some voids, relict rhombic shapes were seen (Fig. 7Ç5b,c), suggesting that the precursor substance was ground magnesite. Scarce, fine sepiolite fibers were seen forming over the stevensite substrate (Fig. 7Ç5c,d).

Chemical Analyses

Major elements. Chemical analyses (Table 1) were performed on the samples collected from the magnesite+sepiolite vein (Fig. 1b,c,d), monomineralic sepiolite (Ç4), and stevensite (Ç5) samples. In the magnesite+sepiolite samples, SiO_2 exhibited a negative correlation with MgO, by increasing contents of SiO_2 from 5.037 to 15.675% and decreasing contents of MgO from 46.134 to 36.184%. This indicated that the sepiolite/magnesite ratio increased from Ç1 to Ç3 (Table 1). Only small amounts of other element oxides were present.

Pure sepiolite consisted of 55.955% SiO_2 and 23.875% MgO in the raw state (Table 1Ç4). The remaining elements were below detection limits. The structural formula calculated per half unit cell (32 oxygen atoms) for sepiolite was: $(Ca_{0.02}Na_{0.01}K_{0.01})(Mg_{7.68}Al_{0.08}\square_{0.24})Si_{12.08}O_{30}(OH)_4$. After correction, assigning the excess SiO_2 to quartz (0.08 atoms), the following formula was obtained: $(Ca_{0.05}K_{0.02})(Mg_{7.79}Al_{0.10}\square_{0.11})Si_{12}O_{30}(OH)_4$. In this formula, Mg was the dominant cation. A small amount of Al substituted for Mg in the octahedral positions. The number of structural vacancies (shown by the square symbol) was 0.11 cations per half formula unit (p.h.f.u.).

In chemical analyses of stevensite (Table 1, Ç5), the principal element oxide constituents were SiO_2 and MgO, 50.043% and 16.211%, respectively. The amounts of Al_2O_3 and Fe_2O_3 were larger than those of sepiolite. Except for Na_2O (1.283%), the amounts of interlayer cations were small.

To detect the chemical changes along a line perpendicular to the lamination, spot EMP analyses were performed (Table 2). Element oxides of the major elements in six separate samples were similar. Note that the amounts of Fe_2O_3 and Al_2O_3 found were similar to those obtained by ICP-OES (Table 1, Ç5).

Free iron oxide was removed using the citrate-bicarbonate-dithionite procedure (Mehra and Jackson 1960). At the end of the procedure, due to the presence of Fe^{2+}, the color of both supernatant solution and solid residue appeared green. The green color of the residue corresponded to reduction of structural Fe to Fe^{2+} also indicating that the Fe in the stevensite structure existed initially in ferric form (Fe^{3+}) (Kodama et al. 1988). The ICP-MS analyses of the supernatant solution revealed that free Fe was <1 wt.%. This suggests that almost all of the Fe was present in the crystal structure of stevensite. The following structural formula calculated from ICP-OES analyses on the basis of $O_{10}(OH)_2$ was: $(Ca_{0.01}Na_{0.20}K_{0.04})(Mg_{1.90}Al_{0.30}Fe^{3+}_{0.37}Ti_{0.01}\square_{0.43})(Si_{3.93}Al0.07)O_{10}(OH)_2$. Mg was the dominant octahedral cation, with some substitution by Al and Fe. This composition fell within the trioctahedral domain with a total octahedral occupancy of 2.57 p.h.f.u. (Fig. 8) and vacancies being only 0.43 p.h.f.u. Substitution of Al for Si was low at 0.07 p.h.f.u. The charge distribution was as follows: tetrahedral charge = –0.07 and octahedral charge = –0.15, producing a total layer charge of –0.22 p.h.f.u. The layer charge was balanced primarily by Na (0.20 p.h.f.u.) with small amounts of K (0.04) and Ca (0.01) creating an interlayer charge of +0.25 p.h.f.u. The prominent excess charge was generated mainly from the octahedral sheet consistent with stevensite.

Trace and REE elements. Trace elements showed small values in sepiolite-bearing samples with a low sepiolite/magnesite ratio (Table 1Ç1, Ç2). But in sample Ç3, trace element values increased slightly due to the increase in sepiolite content. Trace element analyses showed that, excluding Ni, Cr, Hf, Sr, and Th, the remaining trace elements were more abundant in pure sepiolites (Ç4) than in magnesite+sepiolite. In stevensite (Ç5), Ni, Co, and V values were almost the same as in sepiolite. The remaining trace elements showed considerable enrichment in stevensite compared to sepiolite.

The REE (rare earth elements) values in magnesite-rich samples (Ç1, Ç2) (Table 1) showed enrichment in LREE (light

https://doi.org/10.1007/s42860-020-00083-9 Published online by Cambridge University Press

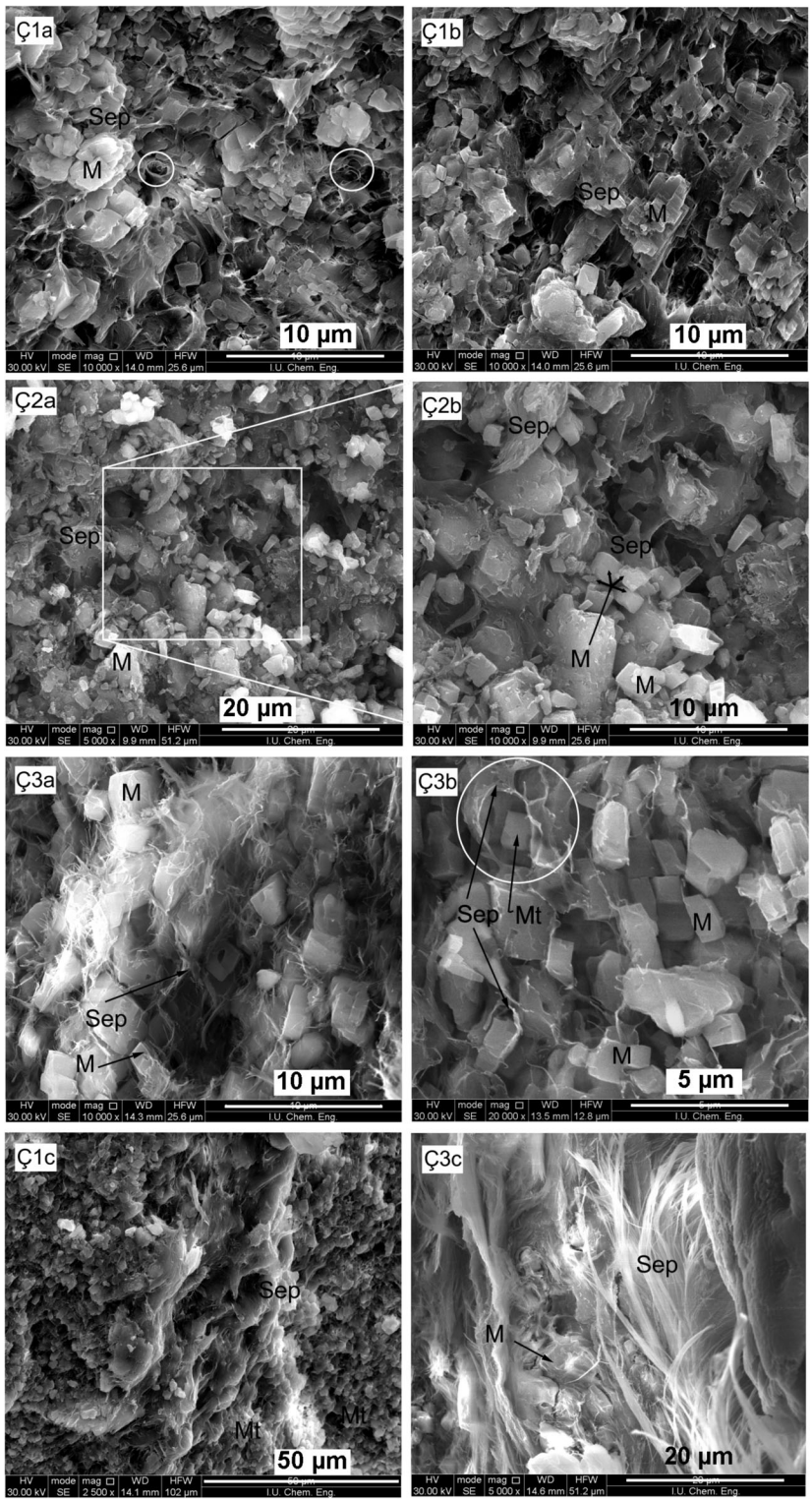

Fig. 6. SEM images from the magnesite+sepiolite vein (Ç1, Ç2, Ç3): sepiolite formed in interstitial space parallel to crystal faces enclosing the magnesite rhombs (Ç1a, 1b, Ç3a). Small magnesite crystal relicts remained at the centers of the voids, indicating that replacement of magnesite by sepiolite was interrupted (Ç1a, Ç2a, 2b, Ç3a, 3b). Where transformation was completed, hollow voids which were embraced by sepiolite display sepiolite pseudomorphs (Ç1a, 1b, Ç3a). Concentric voids (encircled) indicate subsequent replacement stages (1a). Late sepiolite formed in veinlets as parallel fine fibers and flakes (Ç1c, Ç3c). Sep, sepiolite; M, magnesite

https://doi.org/10.1007/s42860-020-00083-9 Published online by Cambridge University Press

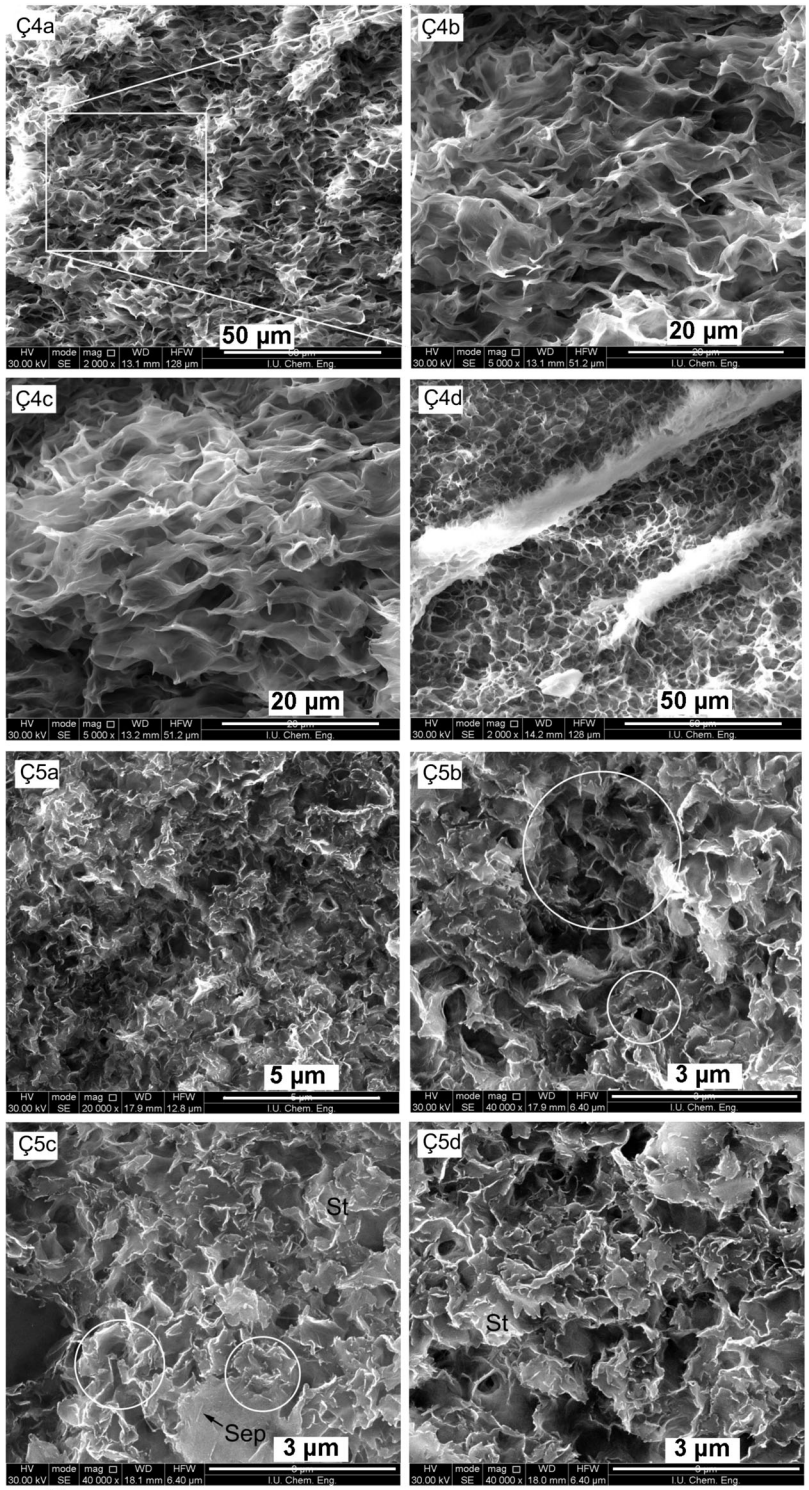

Fig. 7. SEM images of sepiolite (Ç4) and stevensite (Ç5): sepiolite occupies the overall mass as sepiolite pseudomorphs after magnesite forming a net structure (Ç4a–Ç4d). Note that the corners of some voids are rounded, though rhombohedral shapes are clearly seen throughout the sample. Sepiolite formation fills a fine desiccation crack (Ç4d). SEM images of stevensite, parallel (Ç5a, 5b) and perpendicular (Ç5c, 5d) to lamination. Fine, uneven flakes surrounding the voids (Ç5a, 5b, 5d) or large flakes parallel to the surfaces of laminae (Ç5c, 5d). Randomly distributed, irregularly shaped, sub-rounded voids with sizes ranging from 0.1 to 1.5 µm (Ç5a–Ç5d). Relic rhombohedral shapes inherited from precursor magnesite crystals (encircled) (Ç5b, 5c). Scarce sepiolite fibers formed on stevensite substrate (Ç5c). Sep, sepiolite; M, magnesite; St, stevensite

https://doi.org/10.1007/s42860-020-00083-9 Published online by Cambridge University Press

Table 1. Mineral compositions (wt.%), major oxides (wt.%), trace elements, and REE (ppm) of magnesite, magnesite+sepiolite, sepiolite, and stevensite samples

Mineral comp.	$M_{93}Se_7$	$M_{90}Se_{10}$	$M_{78}Se_{22}$	Sep_{100}	St_{100}
Major oxides	Ç1	Ç2	Ç3	Ç4	Ç5
SiO_2	5.037	7.114	15.675	55.955	50.043
TiO_2	0.020	0.022	0.023	0.001	0.092
Al_2O_3	0.165	0.174	0.179	0.318	4.041
Fe_2O_3	0.080	0.104	0.124	0.003	6.214
MnO	0.001	0.002	0.002	0.001	0.028
MgO	46.134	43.346	36.184	23.875	16.211
CaO	0.453	0.468	0.430	0.173	0.064
Na_2O	0.001	0.001	0.001	0.001	1.283
K_2O	0.001	0.001	0.001	0.047	0.442
P_2O_5	0.110	0.127	0.107	0.051	0.234
LOI	49.000	48.600	47.300	19.672	22.344
Total	101.000	99.958	100.025	100.825	100.996
Trace and REE (ppm)					
Ni	4.54	3.51	5.98	2.27	4.59
Cr	17.60	30.53	44.23	27.00	40.33
Sc	2.44	1.95	3.03	24.00	24.00
Ba	7.33	8.07	13.20	28.63	95.33
Co	0.42	0.79	1.84	5.30	5.33
Cs	0.03	0.07	0.10	0.59	5.57
Hf	0.03	0.01	0.19	0.08	20.53
Nb	0.01	0.05	0.23	0.49	65.00
Rb	0.36	0.31	0.52	6.43	9.47
Sr	18.93	18.53	20.87	6.00	44.33
Ta	0.05	0.02	0.03	0.05	5.37
Th	0.34	0.04	0.17	0.00	2.00
U	0.08	0.08	0.55	3.43	6.57
Pb	2.60	2.41	6.53	46.33	60.33
V	30.63	29.80	34.30	46.67	38.00
Zr	0.64	1.68	3.00	2.43	70.00
Y	0.13	0.03	0.11	0.15	11.73
La	0.14	0.11	0.15	0.08	3.57
Ce	0.09	0.16	0.46	0.76	29.43
Pr	0.23	0.17	0.48	0.08	18.73
Nd	0.29	0.15	0.24	0.23	20.80
Sm	0.09	0.07	0.11	0.17	4.77
Eu	0.00	0.00	0.00	0.00	0.18
Gd	0.00	0.04	0.02	0.47	2.20
Tb	0.00	0.00	0.00	0.03	0.38
Dy	0.01	0.01	0.05	0.04	1.74
Ho	0.01	0.00	0.01	0.32	0.07
Er	0.02	0.00	0.01	0.65	0.14
Tm	0.01	0.00	0.00	0.26	0.01
Yb	0.03	0.00	0.05	1.50	0.14
Lu	0.00	0.00	0.02	0.20	0.03
REE	3.36	2.66	4.63	28.79	106.19
LREE	3.19	2.54	4.36	25.15	96.53
HREE	0.17	0.12	0.27	3.6	9.66

M, magnesite; Sep, sepiolite; St, stevensite

https://doi.org/10.1007/s42860-020-00083-9 Published online by Cambridge University Press

Table 2. EMPA analyses of principal element oxides of stevensite (wt.%)

	1*	2	3	4	5	6
SiO_2	58.23	57.90	57.53	57.69	57.45	57.81
Al_2O_3	4.42	4.29	4.39	4.24	4.38	4.35
ΣFeO	6.26	6.03	6.01	5.37	6.46	5.88
MgO	17.70	18.36	17.98	18.49	18.51	19.40
Total	86.61	86.58	85.91	85.79	86.80	87.44

* The numbers 1–6 represent the spots analyzed

rare earth elements), though the HREE (heavy rare earth elements) contents remained low. Excluding La, Pr, Nd, Eu, and Dy, the remaining REE values increased slightly in pure sepiolite. Note that in stevensite, only Ho, Er, Tm, Yb, and Lu exhibited negative correlations with their counterparts in sepiolite. Ce was the same in both sepiolite and stevensite. Other REE displayed significant depletion in stevensite relative to pure sepiolite. The total REE contents (including Sc and La) of magnesite+sepiolite, pure sepiolite, and stevensite were increased: 3.55 (average), 28.79, and 106.19 ppm, respectively (Table 1).

Chondrite-normalized REE patterns of magnesite+sepiolite and stevensite (Fig. 9) showed large negative anomalies and distinct enrichment in LREE and HREE. Magnesite+sepiolite samples were enriched in Pr, but depleted in other REE elements relative to chondrite. The sepiolite showed enrichment in G. Cerium, Sm, and Lu values were equal to those in chondrite, but the sepiolite was depleted in the remaining REE. Excluding Ce and Dy, pure sepiolite was more enriched in REE compared to magnesite+sepiolite samples. Stevensite displayed a different pattern. All REE in stevensite were enriched several times when compared with sepiolite and magnesite+sepiolite.

DISCUSSION

Magnesite

Magnesite was formed by the interaction of CO_2-rich surface waters with serpentinite during ophiolite emplacement (Yeniyol 1982; Tuncay 2000). The CO_2-rich waters reacted with serpentinite involving the decomposition of mafic and felsic minerals. This reaction produced waters rich in Mg, Si, Fe, and trace and REE elements. Magnesium reacted with CO_2 generating magnesite veins (Eq. 1). Iron sesquioxides caused the staining of the serpentinite in light–dark brown colors. Silica appeared as thin veinlets of quartz, chalcedony, or opal traversing both serpentinite and magnesite. Finely disseminated crystallites resulted in silicification of magnesite and serpentinite. Excess silicification and staining with Fe oxides led to the formation of listwanite (iron cap) which could be indicative of the presence of magnesite formation locally.

$$\underset{\text{Serpentinite}}{H_4Mg_3Si_2O_9} + 2H_2O + 3CO_2 \rightarrow \underset{\text{Magnesite}}{3MgCO_3} + 4H_2O + 2SiO_2 \quad (1)$$

Geochemical 'signals' may give clues to different sources (e.g. mafic or felsic rocks), e.g. Zr, Th, and La are scarce in magnesite, indicating ultramafic and mafic rocks as the source rocks. High concentrations of Cr, Ni, Co, V, and Sc support this suggestion. Because of large ion charge and large ionic radii, incompatible REE ions cannot participate in isomorphic substitution in ferromagnesian minerals. As a consequence, ultramafic rocks and serpentinite are REE-poor. REE are also incompatible with respect to participation in ionic substitution with Mg ions in the rhombohedral structure of magnesite. Therefore, magnesite contains very little in terms of REE, indicating a genetic relationship with the ultramafic and mafic source rocks (e.g. serpentinite and gabbro) (Table 1). Trace elements are concentrated in accessory mineral phases whereas REE are concentrated in trace carbonate phases (excluding magnesite) which are frequently found in magnesite or in clay minerals (Möller 1989).

Sepiolite

The XRD data indicated that the current sepiolite was poorly ordered. The 110 reflection appeared with a *d* value of 12.64 Å in bulk samples which was considerably larger than those previously documented as poorly ordered sepiolite (Yeniyol and Öztunalı 1985; Yeniyol 1986, 1993; Ece and Çoban 1994; Yalçın and Bozkaya 1995; Chahi et al. 1997; Ece 1998). Excluding the 110 reflection, which was relatively sharp and more intense, the characteristics of the other reflections were similar to those of sepiolite-13 Å (Yeniyol 2014).

The SEM observations displayed clear evidence that sepiolite was formed at the expense of magnesite. Magnesite dissolution began from crystal faces and continued towards the core as seen in the samples of magnesite+sepiolite. Subsequently, sepiolite grew in interstitial space making sepiolite walls that enveloped the magnesite crystals (Fig. 6Ç3a, b). Ongoing dissolution led to decreasing size of the magnesite crystals, thickening of the sepiolite walls, and rounding of the corners by adding newly formed sepiolite. When the transformation mechanism was interrupted, relicts of magnesite crystals remained in the centers of the voids (Fig. 6Ç2b, Ç3b). In samples where magnesite crystals were replaced entirely, sepiolite walls surrounded the voids with roughly rhombic shapes. These voids represented the remnants of former magnesite crystals displaying sepiolite pseudomorphs after magnesite (Fig. 6Ç1b). In these samples, voids with almost rhombic outlines formed a net structure consisting of pure sepiolite.

Sepiolite and stevensite were formed after magnesite. Sepiolite appeared locally in a stockwork magnesite deposit. It replaced the entire mass of thin magnesite veins. Sepiolite was also found together with magnesite in a thick vein consisting of both magnesite and sepiolite (magnesite+sepiolite). The sepiolite content increased regularly from the center toward the surfaces and from the bottom to the top of the vein. In addition to field observations, XRD analyses, SEM, and chemical analyses also supported such an increment, suggesting sepiolite formation was achieved by descending surface waters. Mineral compositions which were calculated from ICP-OES analyses (Table 1Ç1–Ç3) also confirmed a regular increase in sepiolite contents from the base toward the top in the order of 7, 11, and 22 wt.%.

https://doi.org/10.1007/s42860-020-00083-9 Published online by Cambridge University Press

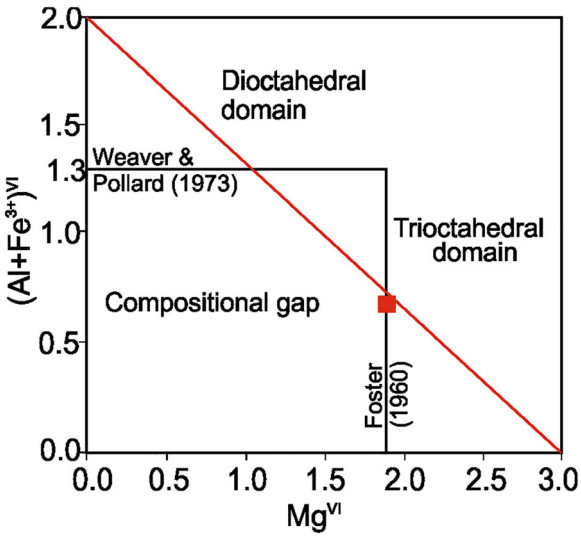

Fig. 8. $(Al+Fe^{3+})^{IV}$ vs. Mg diagram showing the compositional variation of smectites. □ indicates the position of stevensite from the present study (Foster 1960; Weaver and Pollard 1973)

In pure sepiolite samples, the principal element oxides were SiO_2 and MgO with contents of 55.955% and 23.875%, respectively. The remaining oxides were below detection limits. In this respect, sepiolite showed an ideal chemical composition. Except for Ni, Cr, Hf, Sr, Ta, and Th, sepiolite was enriched with the remaining trace elements which were adsorbed from descending solutions (Table 1). Of the HREE, Ho, Er, Tm, Yb, and Lu were absorbed and showed little in terms of enrichment compared to magnesite. The remaining REE were as low as in the magnesite. Sepiolite was enriched in trace elements and REE by nearly six times more than magnesite.

Field relationships, supported by analytical data, revealed that sepiolite was transformed from magnesite by descending waters of surface origin. These waters were Si-rich, containing Fe and Al as well as trace and REE elements. Waters of this nature were derived from the supergene alteration of ultramafic rocks consisting of serpentinite and gabbro dykes. Si-rich surface waters reacted with magnesite under very low Al and

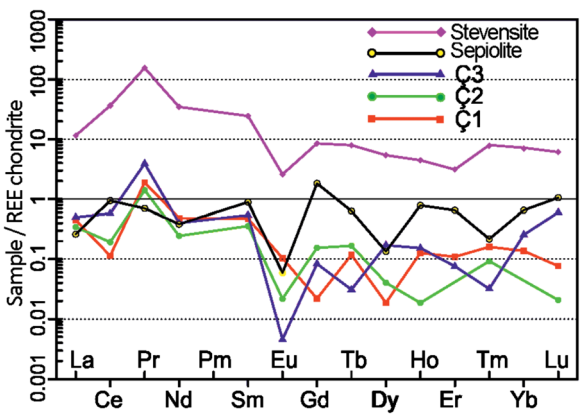

Fig. 9. Chondrite-normalized REE pattern of the samples investigated (normalization values from Boynton 1984)

Fe and high Si and Mg activities with pH values ranging between 8.0 and 9.5 (Wollast et al. 1968; Khoury et al. 1982; Galan and Castillo 1984; Abtahi 1985; Jones and Galan 1988; Galan and Pozo 2011). Under these physicochemical conditions, magnesite was transformed to sepiolite. Quartz veinlets crosscutting the sepiolite veins indicated a high activity of SiO_2 which favored the formation of sepiolite (Birsoy 2002). These waters replaced the relatively soft and friable magnesite in situ via a dissolution–precipitation mechanism. This event became less effective from top to base, and from vein surfaces toward the inner parts in thick magnesite veins. In the case of thin veins (stockwork magnesite), magnesite was entirely replaced leaving behind pure sepiolite. The probable reaction resulting in sepiolite formation is given as:

$$\underset{\text{Magnesite}}{8MgCO_3} + 12H_4SiO_4 + 18H_2O \rightarrow \underset{\text{Sepiolite}}{Mg_8Si_{12}O_{30}(OH)_4(OH_2)_4.8H_2O} + 16CO_2 + 2H_2O + 16(OH)^- \quad (2)$$

Stevensite

The SEM analyses indicated that stevensite occupied the overall mass by the transformation mechanism similar to the sepiolite. No remnant of precursor mineral was detected. Stevensite appeared as wavy flakes and packets which were formed in intergranular space surrounding the voids. This appearance was different from the 'honeycomb structure' which appears frequently in smectites. In fact, the voids were irregularly shaped, sub-rounded with sizes ranging from 0.1 to 1.5 μm, and showing random spatial distribution. These features indicated a pre-existing mylonitized material from which stevensite was formed. Some rare voids with relict rhombic outlines indicated that the precursor material was magnesite. In support of field observations, SEM data demonstrated that mylonitized magnesite was replaced completely by stevensite.

Stevensite appeared within a gallery bordered above and below by a thick magnesite vein. The magnesite vein underwent tectonism resulting in it breaking in two, crushing and grinding, and as a consequence forming a mylonitic zone between these two parts. Stevensite occurred as a horizontal layer replacing the overall mass of mylonitized magnesite. The boundaries between stevensite and magnesite, and between stevensite and the wall-rock serpentinite, were sharp. No evidence of alteration was observed along the latter two borders, suggesting the formation of stevensite from serpentinite.

The principal element oxide constituents were SiO_2 and MgO at 50.043% and 16.211%, respectively. The amounts of Al_2O_3 and Fe_2O_3 were much greater than those of the sepiolite. Aluminum and Fe substituted for Mg in the octahedral sheet whereas little Al substituted for Si in the tetrahedral sheet. These substitutions resulted in an increase in the layer charge on the tetrahedral, but mainly on the octahedral sheets, which was indicative of stevensite. On the other hand, the $(Al+Fe^{3+})^{IV}$/Mg ratio was greater than that of ideal stevensite. This fact was previously suggested as indicating that some discrete clay mineral layers could be present (Mayayo et al. 2000; Hover and Ashley 2003; Cuevas et al. 2003); however, no indication of such a discrete mineral was detected using XRD and FTIR. According to Foster (1960) and Weaver and Pollard (1973), the Mg and $(Al+Fe^{3+})^{IV}$

https://doi.org/10.1007/s42860-020-00083-9 Published online by Cambridge University Press

contents of the present stevensite were 1.9 and 0.67 p.h.f.u., respectively. Stevensite fell within the trioctahedral domain (Fig. 8). The Mg-smectite classification was made on the basis of the basis of the preferential location of the excess layer charge (Güven 1988). Localization of the layer charge and XRD data, obtained by using the identification procedure of Christidis and Koutsopoulou (2013), demonstrated the presence of stevensite.

Stevensite was formed from fine-grained material (mylonite) which was more vulnerable to alteration than massive and non-disintegrated magnesite. A laminated layer structure suggested that stevensite was formed under a permanent underground water level. Si, Fe, and Al as well as trace elements and REE were sourced mainly from serpentinite. In addition, the presence of additional elements such as Ba, Rb, and Sr could be attributed to the overlying alkaline Neogene lacustrine sediments. The REE are known as insoluble elements; however, their solubility can be raised due to saline conditions which might have been provided by descending alkali solutions generated from surface waters. These elements were accumulated in groundwater via downward movement of surface waters. Stevensite was formed by in situ transformation from mylonitized magnesite by Si-rich solutions via a dissolution–precipitation mechanism in the groundwater environment (Eq. 3). A small amount of free Fe acted as a staining agent which made the lamination apparent, but most of the Fe was incorporated into the crystal structure together with Al. All trace elements participated in stevensite formation. Excluding Co, Sc, and V, the remaining trace elements showed several-fold enrichments in stevensite compared to sepiolite. Of the HREE, only Ho, Er, Tm, Yb, and Lu exhibited negative correlations with their counterparts in sepiolite (Table 1). During stevensite formation, REE were removed from solution under water where these elements were enriched.

The physicochemical conditions were: high Mg+Fe/Si ratios, high-alkali salinity, and higher pH (>9.5) than that required for sepiolite formation (Siffert 1962; Jones and Galan 1988; Birsoy 2002). These conditions were responsible for the transformation of magnesite to stevensite. The probable chemical reaction is given as:

$$\underset{\text{Magnesite}}{6MgCO_3 + 8H_4SiO_4 + 6H_2O \rightarrow} \quad \underset{\text{Stevensite}}{2Mg_3Si_4O_{10}(OH)_2.4H_2O + 16H_2O + 6CO_2} \qquad (3)$$

CONCLUSIONS

Two daughter minerals, sepiolite and a newly found stevensite, appeared locally in a magnesite deposit at Çayırbağı displaying an unusual mode of occurrence and genetic relationships with magnesite.

Sepiolite either replaced the entire mass of thin magnesite veins or is found together with magnesite in a thick vein consisting of both magnesite and sepiolite. Sepiolite was poorly ordered, showing large d_{110} reflections appearing at 12.64 Å and 13 Å in air dried and ethylene glycolated states, respectively. The characteristics of the remaining reflections, as well as its structural, crystal chemical, thermal, and textural properties, indicated that this sepiolite is poorly ordered and is present as the sepiolite-13 Å form.

Stevensite appeared inside a gallery occupying a mylonitized zone between two parts of a thick magnesite vein. The d_{001} reflection appeared at 14.7 Å in the air-dried state and at 18.3 Å when solvated with ethylene glycol. The structural, thermal, and textural properties were similar to those of Mg-smectites. The stevensite had unusually large Fe and Al contents. The layer-charge localization and XRD data demonstrated that this mineral is an Fe- and Al-rich stevensite.

Sepiolite and stevensite were formed by in situ transformation of the magnesite parent mineral via a dissolution–precipitation mechanism involving the replacement of pre-existing magnesite. Various physicochemical conditions were instrumental in their formation. Supergene alteration of ultramafic rocks (serpentinite and gabbro) yielded waters with high Si as well as low Al and Fe activities, and contained trace elements and REE in small amounts.

Sepiolite was formed by the descending waters of this nature reacting with magnesite under pH values of 8–9.5. Sepiolite was formed stepwise, by replacing the pre-existing magnesite. Due to the increasing sepiolite content, trace elements and REE were also enriched by means of absorption, albeit in small amounts.

Differing from sepiolite, stevensite was formed by transformation from magnesite under the permanent groundwater level, where Si, Fe, Al, trace elements, and REE were considerably enriched via descending waters. Si activity lower than that required for the formation of sepiolite, high Al and Fe activities, and pH values of >9.5 were decisive environmental factors leading to the production of stevensite. Trace and REE participated in and enriched stevensite formation by means of absorption from the REE-rich groundwater.

ACKNOWLEDGMENTS

The author thanks B. Arman (Turkey Bottle and Glass Factory Research Center) for the EMP analyses, S.K. Pabucçuoğlu (Istanbul University-Cerrahpaşa, Department of Chemistry) for the FTIR analyses, C. Kahruman (Istanbul University-Cerrahpaşa, Department of Metallurgical and Materials Engineering) for the thermal analyses, M.A. Gürkaynak (Istanbul University-Cerrahpaşa, Department of Chemistry) for the SEM analyses, and N. Aysal (Istanbul University-Cerrahpaşa, Department of Geology) for the LA-ICP-MS and ICP-OES analyses. Thanks also to Joseph. W. Stucki, Editor-in-Chief, and Selahattin Kadir, Associate Editor, for their valuable editorial comments and suggestions. Anonymous reviewers are thanked for their careful reviews and comments which helped to improve the manuscript.

Compliance with Ethical Standards

Conflict of Interest

The authors declare that they have no conflict of interest.

https://doi.org/10.1007/s42860-020-00083-9 Published online by Cambridge University Press

REFERENCES

Abtahi, A. (1985). Synthesis of sepiolite at room temperature from SiO_2 and $MgCl_2$ solution. *Clays and Clay Minerals, 20*, 521–523.

Akbulut, A., & Kadir, S. (2003). The geology and origin of sepiolite and palygorskite and stevensite in Neogene lacustrine sediments of the Serinhisar-Acıpayam basin, Denizli, SW Turkey. *Clays and Clay Minerals, 51*, 279–292.

April, R. H., & Keller, D. M. (1992). Saponite and vermiculite in amygdales of the Granby basaltic tuff, Connecticut valley. *Clays and Clay Minerals, 40*, 22–31.

Benhammou, A., Tanouti, B., Nibov, L., Yacoubi, A., & Bonnet, J. (2009). Mineralogical and physicochemical investigation of Mg-smectite from Jbel Ghassoul, Morocco. *Clays and Clay Minerals, 57*, 264–270.

Birsoy, R. (2002). Formation of sepiolite-palygorskite and related minerals from solution. *Clays and Clay Minerals, 50*, 736–745.

Boynton, W. V. (1984). Geochemistry of rare earth elements: Meteorite studies. In P. Henderson (Ed.), *Rare Earth Element Geochemistry* (pp. 63–114). New York: Elsevier.

Buey, C. S., Barrios, M. S., Romero, E. G., & Montoya, M. D. (2000). Mg-rich smectite "precursor" phase in the Tagus basin, Spain. *Clays and Clay Minerals, 48*, 366–373.

Chahi, A., Fritz, B., Duplay, J., Weber, F., & Lucas, J. (1997). Textural transition and genetic relationship between precursor saponite and sepiolite in lacustrine sediments (Jbel Rhassoul Morocco). *Clays and Clay Minerals, 45*, 378–389.

Christidis, G. E., & Mitsis, I. (2006). A new Ni-rich Saponite from the ophiolites complex of Othrys, Central Greece. *Clays and Clay Minerals, 54*, 653–666.

Christidis, G. E., & Koutsopoulou, E. (2013). A simple approach to the identification of trioctahedral smectites by X-ray diffraction. *Clay Minerals, 48*, 687–696.

Cuevas, J., Vigil de la Villa, R., Ramirez, S., Petit, S., Meunier, A., & Leguey, S. (2003). Chemistry of Mg smectites in lacustrine sediments from the Vicalvaro sepiolite deposit, Madrid Neogene basin (Spain). *Clays and Clay Minerals, 51*, 457–472.

Eberl, D. D., Jones, B. F., & Khoury, H. N. (1982). Mixed layer kerolite–stevensite from the Amargosa Desert, Nevada. *Clays and Clay Minerals, 30*, 321–326.

Ece, Ö. I. (1998). Diagenetic transformation of magnesite pebbles and cobles to sepiolite (meerschaum) in the Miocene Eskişehir lacustrine basin, Turkey. *Clays and Clay Minerals, 46*, 436–445.

Ece, Ö. I., & Çoban, F. (1994). Geology, occurrence and genesis of Eskişehir sepiolites, Turkey. *Clays and Clay Minerals, 42*, 81–92.

Elton, N. J., Hooper, J. J., & Holyer, A. D. (1997). An occurrence of saponite and kerolite in the Devonian Cruosa gabbro at Dean Quarry, The Lizard, Cornwall, England. *Clay Minerals, 32*, 241–252.

Faust, G. T., & Murata, K. J. (1953). Stevensite, redefined as a member of the montmorillonite group. *American Mineralogist, 38*, 973–987.

Foster, M. (1960). Interpretation of the composition of trioctahedral micas. *US Geological Survey Professional Paper, 354-B*, 11–50.

Frost, R. L., & Ding, Z. (2003). Controlled rate thermal analysis and differential scanning calorimetry of sepiolites and palygorskites. *Thermochimica Acta, 397*, 119–128.

Frost, R. L., Cash, G. A., & Kloprogge, T. H. (1998). Rocky Mountain leather, sepiolite and attapulgite – an infrared emission spectroscopic study. *Vibrational Spectroscopy, 16*, 173–184.

Frost, R. L., Locos, O. B., Ruan, H., & Kloprogge, T. H. (2001). Near-infrared and mid-infrared spectroscopic study of sepiolites and palygorskites. *Vibrational Spectroscopy, 27*, 1–13.

Furquim, S. A. C., Graham, R. C., Barbiero, L., Neto, J. P. Q., & Valles, V. (2008). Mineralogy and genesis of smectites in alkaline-saline environment of Pantanal wetland, Brasil. *Clays and Clay Minerals, 56*, 579–595.

Galan, E. & Castillo, A. (1984). Sepiolite-Palygorskite in Spanish Tertiary Basins; genetic patterns in continental environments. Pp. 87–124 in: *Palygorskite-Sepiolite Occurrences, Genesis and Uses* (A. Singer and E. Galan, editors). Developments in Sedimentology, 37, Elsevier, Amsterdam.

Galan, E. & Pozo, M. (2011). Palygorskite and sepiolite deposits in continental environments. Description, genetic patterns and sedimentary settings. Pp. 125–173 in: *Developments in Palygorskite-Sepiolite Research. A New Outlook on these Nanomaterials* (E. Galan and E. Singer, editors). Developments in Clay Science, 3, Elsevier, Amsterdam.

Güven, N. (1988). Smectites. Pp. 497–559 in: *Hydrous Phyllosilicates (Exclusive of Micas)* (S.W. Bailey editor). Reviews in Mineralogy, *19*, Mineralogical Society of America, Washington DC, USA.

Hover, W. C., & Ashley, G. M. (2003). Geochemical signatures of paleo depositional environments: ASTEM/AEM study of authigenic clay minerals from an arid rift basin, Olduvai Gorge, Tanzania. *Clays and Clay Minerals, 51*, 231–251.

Imai, N., Otsuka, R., Nakamura, T., & Tsunashima, A. (1970). Saponite from the Akatani mine, Niigata Perfecture, Northeastern Japan. *Clay Science, 4*, 11–29.

İrkeç, T., & Ünlü, T. (1993). An example to sepiolite formation in volcanic belts by hydrothermal alteration: Kıbrısçık (Bolu). sepiolite occurrence. *Bulletin of the Mineral Research and Exploration, 115*, 49–68.

Jones, B.F. & Galan, E. (1988). Sepiolite and palygorskite. Pp. 631–374 in: *Hydrous Phyllosilicates (Exclusive of Micas)* (S.W. Bailey, editor). Reviews in Mineralogy, *19*, Mineralogical Society of America, Chantilly, Virginia, USA.

Kadir, S., & Akbulut, A. (2001). Occurrence of sepiolite in the Hırsızdere sedimentary magnesite deposit, Bozkurt-Denizli, SW Turkey. *Carbonates and Evaporites, 14*, 191–199.

Kadir, S., Baş, H., & Karakaş. (2002). Origin of sepiolite and loughlinite in a Neogene volcano-sedimentary lacustrine environment, Mihalıççık-Eskişehir, Turkey. *The Canadian Mineralogist, 40*, 191–1102.

Kadir, S., Erkoyun, H., Eren, M., Huggett, J., & Nalgil, N. (2016). Mineralogy, geochemistry, and genesis of sepiolite and palygorskite in Neogene lacustrine sediments, Eskişehir province, West Central Anatolia, Turkey. *Clays and Clay Minerals, 64*, 145–166.

Kadir, S., Eren, M., İrkeç, T., Erkoyun, H., Külah, T., Önalgil, N., & Hugget, J. (2017). An approach to genesis of sepiolite and palygorskite in lacustrine sediments of the Lower Pliocene Sakarya and Porsuk formations in the Sivrihisar and Yunusemre-Biçer regions (Eskişehir, Turkey). *Clays and Clay Minerals, 64*, 310–328.

Karakaş, Z., & Kadir, S. (1998). Mineralogical and genetic relationships between carbonate and sepiolite-palygorskite formations in the Neogene lacustrine Konya basin, Turkey. *Carbonates and Evaporites, 13*, 198–206.

Karakaya, N., Karakaya, M. N. Ç., Temel, A., Küpeli, S., & Tunoğlu, C. (2004). Mineralogical and chemical characterization of sepiolite occurrences at Karapınar (Konya basin, Turkey). *Clays and Clay Minerals, 52*, 495–509.

Khoury, H. N., Eberl, D. D., & Jones, F. B. (1982). Origin of magnesium clays from the Amargosa desert, Nevada. *Clays and Clay Minerals, 30*, 327–336.

Kodama, H., De Kimpe, C. R., & Dejou, J. (1988). Ferrian saponite in a gabbro saprolite at Mont Megantic, Quebec. *Clays and Clay Minerals, 36*, 102–110.

Liu, Y. S., Hu, Z. C., Gao, S., Gunther, D., Xu, J., Gao, C. G., & Chen, H. H. (2008). In situ analysis of major and trace elements of anhydrous minerals by LA-ICP-MS without applying an internal standard. *Chemical Geology, 257*, 34–43.

Mayayo, M. J., Bauluz, B., & Gonzalez Lopez, J. M. (2000). Variations in chemistry of smectites from the Calatayud Basin (NE Spain). *Clay Minerals, 35*, 365–374.

Mehra, O. P., & Jackson, M. L. (1960). Iron oxide removal from soils and clays by a dithionite-citrate system buffered with sodium bicarbonate. Clays and Clay Minerals. *Proc. Natl. Conf. Clays and Clay Minerals, 7*(1958), 317–327.

Möller, P. (1989). Minor and trace elements in magnesite. *Monograph Series on Mineral Deposits, 28*, 173–195.
Nagata, H., Shimoda, S., & Sudo, T. (1974). On dehydration of bound water of sepiolite. *Clays and Clay Minerals, 22*, 285–293.
Papke, K. G. (1972). A sepiolite-rich playa deposit in southern Nevada. *Clays and Clay Minerals, 20*, 211–215.
Post, J. L. (1984). Saponite from Ballarat, California. *Clays and Clay Minerals, 32*, 147–153.
Pozo, M., & Casas, J. (1999). Origin of kerolite and associated Mg clays in palustrine-lacustrine environments. The Esquivias deposit (Neogene Madrid Basin, Spain). *Clay Minerals, 34*, 395–418.
Randal, B. A. O. (1959). Stevensite from Whinn Sill in the region of the North Tyne. *Mineralogical Magazine, 32*, 218–225.
Rautureau, M., & Mifsud, A. (1977). Etude par microscope electronique des differents etats d'hydration de la sepiolite. *Clay Minerals, 12*, 309–318.
Sabah, E., & Çelik, M. S. (2002). Interaction of pyridine derivatives with sepiolite. *Journal of Colloid and Interface Science, 251*, 33–38.
Serna, C., Ahlrichs, J. L., & Serratosa, J. M. (1975). Folding in sepiolite crystals. *Clays and Clay Minerals, 23*, 452–427.
Siffert, B. (1962). Quelques reactions de la silice en solution; La formation des argiles. *Memoires du Service de la Carte Geologique d'Alsace-Lorraine, 21*, 100 pp.
Singer, A., Stahr, K., & Zarei, M. (1998). Characteristics and origin of sepiolite (Meerschaum) from Central Somalia. *Clay Minerals, 33*, 349–362.
Stoessell, R. K., & Hay, R. L. (1978). The geochemical origin of sepiolite and kerolite at Amboseli, Kenya. *Contributions to Mineralogy and Petrology, 65*, 255–267.
Suarez, M., & Garcia-Romero, E. (2006). FTIR spectroscopic study of palygorskite: Influence of the composition of the octahedral sheet. *Applied Clay Science, 31*, 154–163.
Tettenhorst, R., & Moore, G. E. (1978). Stevensite oolites from Green River formation, Central Utah. *Journal of Sedimentary Petrology, 48*, 587–594.
Tuncay, A. (2000). On the origin of the Çayırbağı-Meram (Konya) magnesite deposits. *Geological Bulletin of Turkey, 43*, 21–31.
Weaver, C.D. & Pollard, L.D. (1973). The Chemistry of Clay Minerals. *Developments in Sedimentology, 15*. Elsevier Scientific Publishing Co., Amsterdam, 213 pp.
Wollast, R., Mackenzie, F. T., & Bricker, D. P. (1968). Experimental precipitation and genesis of sepiolite at earth surface conditions. *American Mineralogist, 53*, 1645–1661.
Wouters, M., Rentrop, C., & Willemsen, P. (2010). Surface structuring and coating performance Novel biocide free nanocomposite coatings with anti-fouling and fouling-release properties. *Progress in Organic Coatings, 68*, 4–11.
Yalçın, H., & Bozkaya, Ö. (1995). Sepiolite and palygorskite from the Hekimhan region (Turkey). *Clays and Clay Minerals, 43*, 705–717.
Yalçın, H., & Bozkaya, Ö. (2004). Ultramafic-rock-hosted vein sepiolite occurrences in the Ankara ophiolitic mélange, Central Anatolia, Turkey. *Clays and Clay Minerals, 52*, 227–239.
Yeniyol, M. (1982). Yunak (Konya) magnezitlerinin oluşum sorunları, değerlendirilmeleri ve yöre kayaçlarının petrojenezi. *İstanbul Yerbilimleri, 3*, 21–51.
Yeniyol, M. (1986). Vein-like sepiolite occurrence as a replacement of magnesite in Konya, Turkey. *Clays and Clay Minerals, 34*, 353–356.
Yeniyol, M. (1992). Geology, mineralogy and genesis of the Yenidoğan (Sivrihisar). sepiolite deposit. *Mineral Research and Exploration Bulletin of Turkey, 114*, 71–84.
Yeniyol, M. (1993). Meerschaum sepiolite and palygorskite occurrence in Central Anatolia, Turkey. Pp. 378–382 in: *Clays: Controlling the Environment*; *Proceedings of 10th International Clay Conference,* Adelaide.
Yeniyol, M. (1997). The mineralogy and economic importance of a loughlinite deposit at Eskisehir, Turkey. Pp. 83–88 in: *Clays: For Our Future; Proceedings of the 11th International Clay Conference*, Ottawa.
Yeniyol, M. (2007). Characterization of a Mg-rich and low-charged saponite from the Neogene lacustrine basin of Eskişehir, Turkey. *Clay Minerals, 42*, 541–548.
Yeniyol, M. (2012). Geology and mineralogy of a sepiolite-palygorskite occurrence from SW Eskişehir (Turkey). *Clay Minerals, 47*, 93–104.
Yeniyol, M. (2014). Characterization of two forms of sepiolite and related Mg-rich minerals from Yenidoğan (Sivrihisar, Turkey). *Clay Minerals, 49*, 91–108.
Yeniyol, M. & Öztunalı, Ö. (1985). Yunak sepiolitinin mineralojisi ve oluşumu. *2. Ulusal Kil Sempozyumu,* s. 171–186, Ankara.

(Received 19 February 2020; revised 26 May 2020; AE: Selahattin Kadir)